Supplement of Atmos. Meas. Tech., 18, 1039–1061, 2025
https://doi.org/10.5194/amt-18-1039-2025-supplement

Atmospheric Measurement Techniques
Open Access
EGU

Supplement of

Comparison of temperature and wind profiles between ground-based remote sensing observations and numerical weather prediction model in complex Alpine topography: the Meiringen campaign

Alexandre Bugnard et al.

Correspondence to: Martine Collaud Coen (martine.collaud@meteoswiss.ch)

S1 Instruments during the Meiringen Campaign

The measurement campaign in Meiringen runs from 13.10.2021 to September 2022. The following instruments were installed:

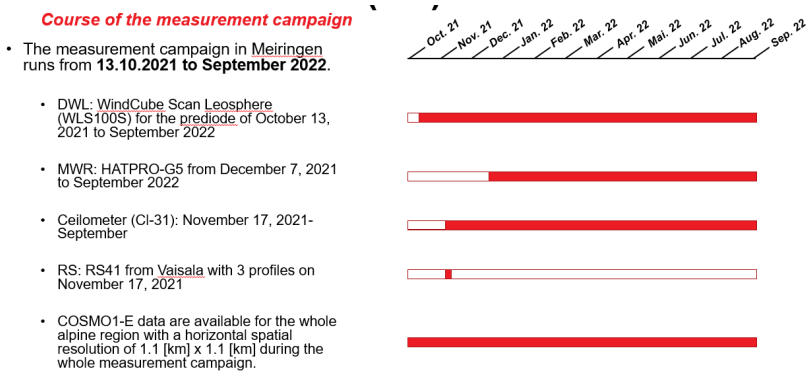

Figure S1. Time line with instruments' presence during the Meiringen Campaign

S2 Topography of KENDA-1

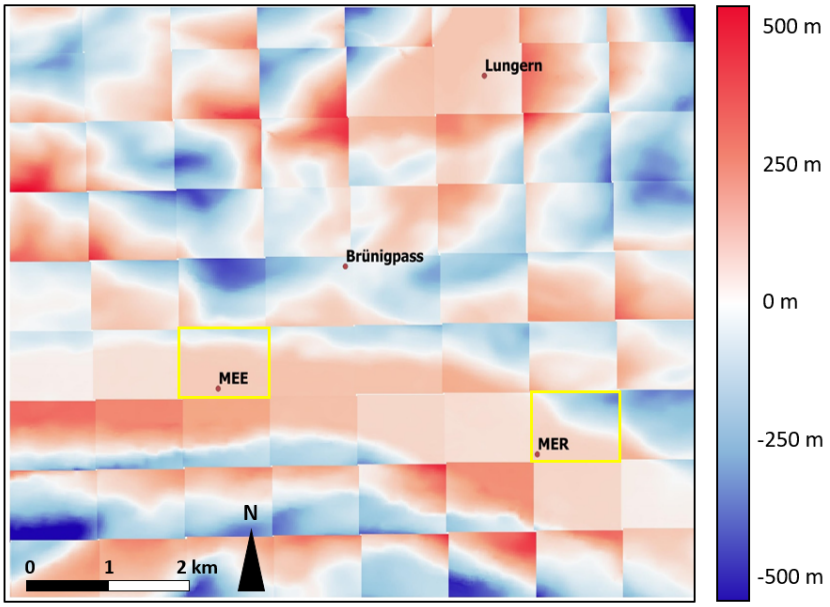

Figure S2. KENDA-1 altitude bias [m] relative to the 25 m resolution digital elevation model in the region of Meiringen. The two used cells are highlighted in yellow.

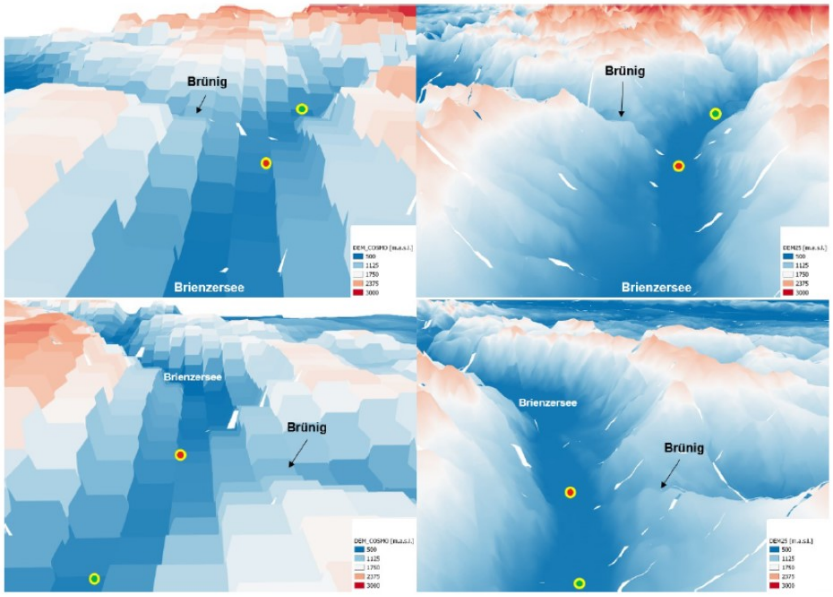

Figure S3. Comparison between KENDA-1 DEM (left) and the DEM25 based on the 1:25'000 Swiss national map for the Haslital valley towards Lake Brienz to the west (bottom) and up the valley (top) to the east. The MEE and MER are represented by the red and green dots, respectively.

S3 MWR vertical resolution

Table S1. Vertical resolution and RMS error (given by the manufacturer) of the MWR temperature according to its different ranges.

Range [m.a.g.l.]	Vertical resolution [m]	RMSE [°C]
0-250	50	0.25
250-500	75	0.25
500-800	100	0.50
800-1200	150	0.50
1200-1600	150	0.75
1600-2200	200	1.00
2200-3000	300	1.00

S4 Weather conditions

Table S2. Absolute values and differences/ratios to the climatic norm (1991-2020) for monthly temperature, total precipitation and proportion of max. sunshine duration in SMN/MER.

	Temp. [°C]		**Precip. [mm]**		**% max sunshine**	
	Abs.	ΔT_{norm}	*Abs.*	*% Norm*	*Abs.*	*% Norm*
Nov	3.1	-0.6	57.8	61.03	38	90
Dec	-1.5	-1	119	121.93	30	90
Jan	-2	-0.9	35	42.42	54	130
Feb	2.2	+1.8	90.5	125.52	54	120
Mar	6.4	+1.4	17.6	20.71	70	150
Apr	8.8	-0.4	74.4	82.85	54	110
May	15.3	+2.1	47.2	34.43	48	110
Jun	18.7	+2.2	142	95.95	53	110
Jul	20.4	+2.5	72.5	45.26	62	130
Aug	19.7	+2.3	89.7	51.49	61	120

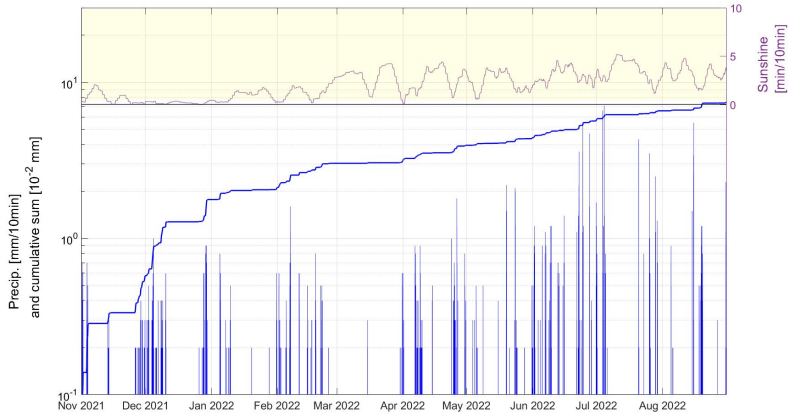

Figure S4. Time series of precipitation intensity [mm/10mm] (blue bar), cumulative precipitation [mm] (blue line) and mean sunshine duration [min/10min] (5 days moving average)

S5 T gradient climatology

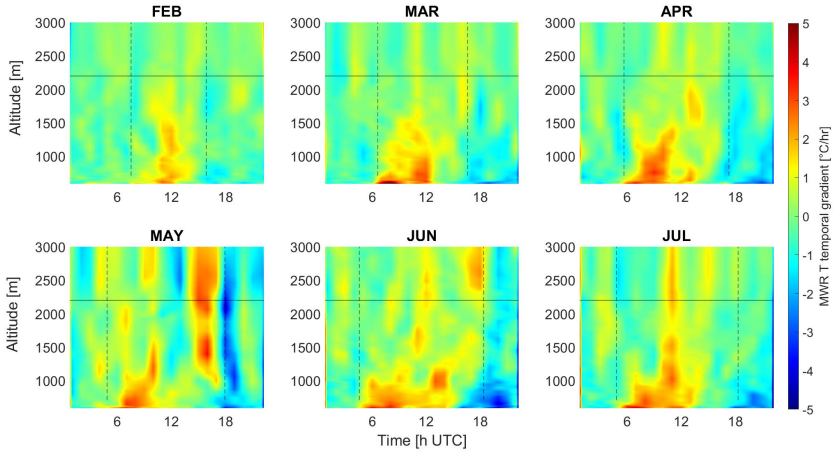

Figure S5. Monthly median of MWR temporal T gradient [°C/hr]. Sunset and sunrise are depicted with the dotted lines.

S6 T-inversion at the end of March

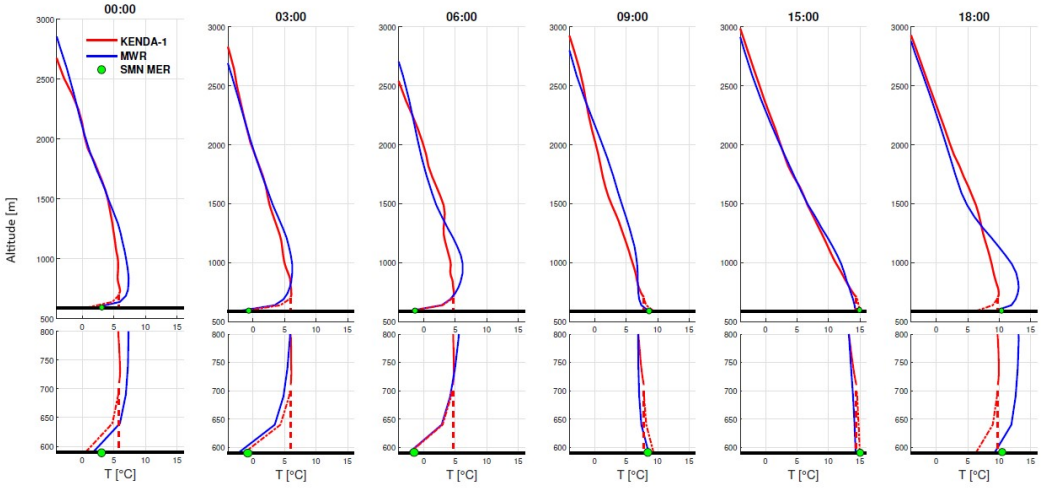

Figure S6. T-profile from MWR (blue) and KENDA-1 (red) for the 22.03.2022. The dashed line indicates the raw value of KENDA-1 as it is used in the ground T comparison. The dash-dotted line extends the profile to the ground with the same gradient as the MWR measurement.

S7 Wind direction profiles as a function of cloud cover

The cloud cover was estimated by the Automatic Partial Cloud Amount Detection Algorithm (APCADA) (Dürr and Philipona, 2004). APCADA uses measurements of longwave downward radiation (LDR), temperature and relative humidity from the SMN stations to estimate the cloud coverage in okta, with a time resolution of 10 min. This algorithm has the disadvantage that high cloud radiating at temperature near the background one (cirrus clouds) are not detected (Pasquier, 2018). We considered that the thermally driven valley winds are mostly dependent on the cloud cover from 2 hours after sunrise to mid-afternoon. We selected than various cloud cover as mean APCADA values at FRU between sunrise + 2 hours and 15h. Fig. S7 presents the results for a mean cloud cover smaller than 5 oktas. Figures similar to Fig. S7 were produced for various cloud cover between 2 to 7 oktas for DWL/MEE. The main features remain similar for all cloud cover apart from i) an increased presence of along valley wind in February with larger cloud cover and ii) the absence of a clear diurnal cycle of along valley wind from the ground to 100 m in August for cloud cover smaller than three oktas.

Dürr, B., and Philipona, R.: Automatic amount detection by surface longwave downward radiation measurements, J. Geophys. Res. 109, DOI: 10. 1029/2003JD004182, 2004. Pasquier, J.: Cloud Cover Detection and its Automation. Internship project at MeteoSwiss, 2018.

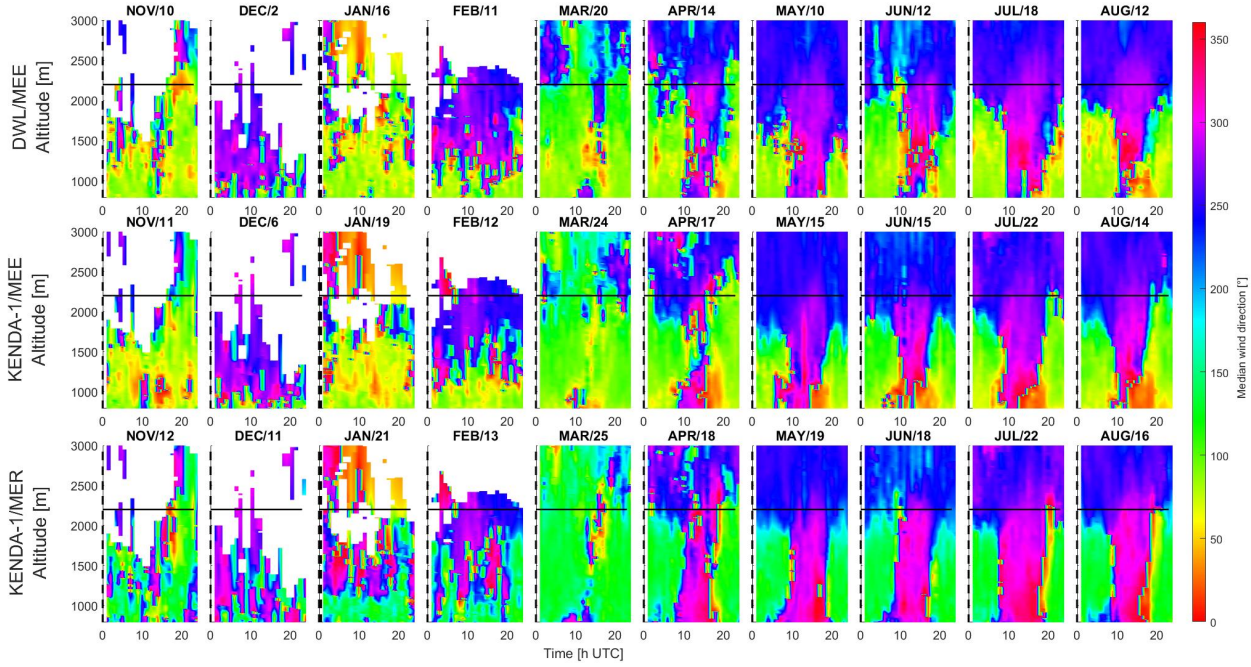

Figure S7. Monthly median wind direction [°] for a) DWL/MEE, b) KENDA-1/MEE and c) KENDA-1/MER (1.11.2001-23.08.2022) for clear weather days. The clear weather days are determined by less than 5 oktas of cloud cover measured at the SMN station of Frutigen (FRU).

S8 Ten year climatology of SMN/MER along valley winds

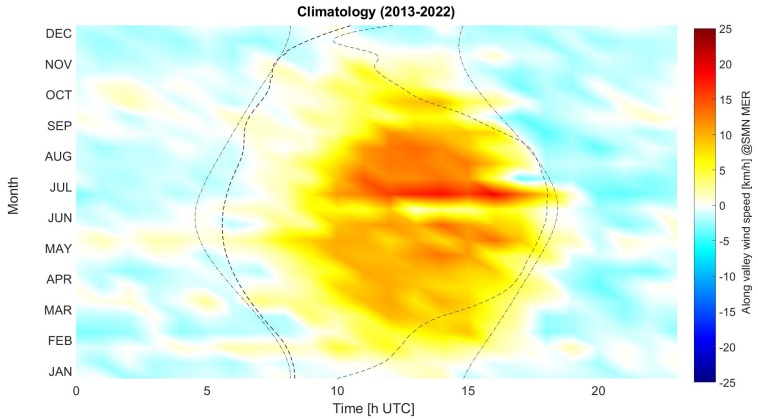

Figure S8. 10 year climatology of seasonal and diurnal cycles of the along-valley wind speeds [km/h] at SMN/MER. Dashed lines correspond to sunrise and sunset times. True sunrise and sunset taking shading into account are represented with the dashed-dotted line.

S9 DWL/MEE radial speeds

S9 is an exemple of the DWL/MEE radial speeds during a hot day in July 2022. Down slope wind from the Brünig Pass are clearly visible and a cross valley circulation above MEE is clearly visible. This cross valley circulation is measured both in case of up and down valley winds and at various time of the day. In the monthly plot (Fig. 9), the cross valley circulation only appears in the late afternoon in April, and from June to August.

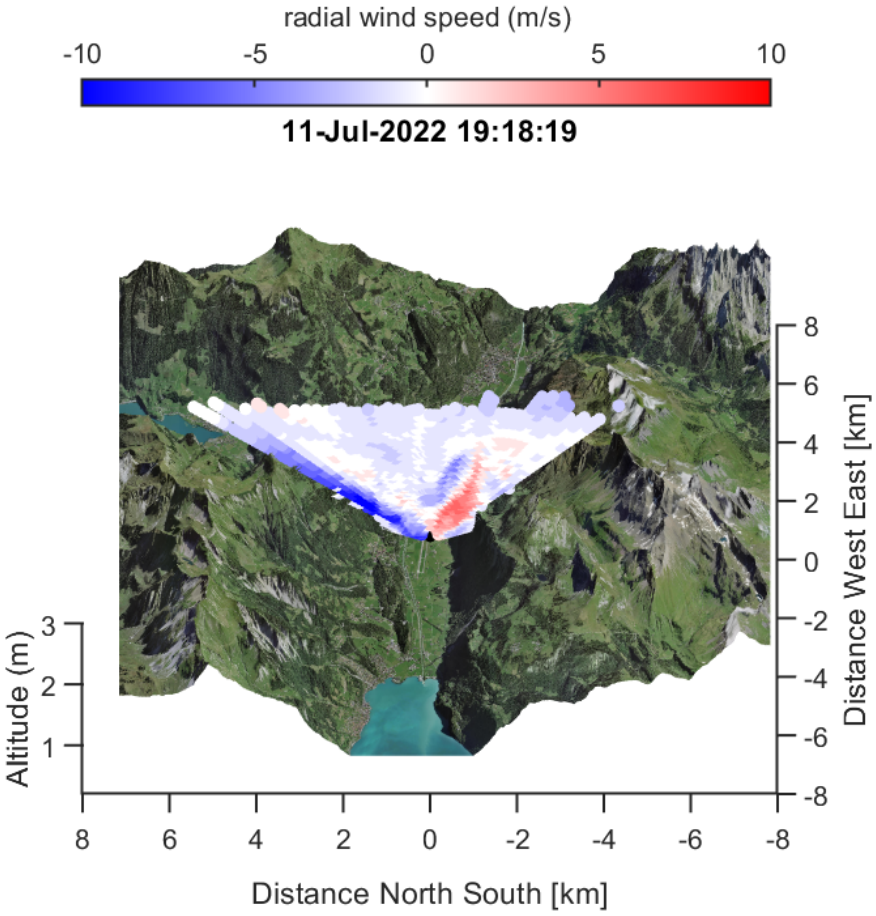

Figure S9. DWL/MEE radial speeds perpendicular to the valley axis on the 11 July 2022 at 19:38:00. The map was downloaded from Swisstopo (https://map.geo.admin.ch, last access on the 31 January 2024)

S10 Wind pattern at SMN stations

All these stations show valley wind patterns from March to August and in November at some stations (MER, BRU, LUN and GIH). The up valley daily period at BRZ und BUC is less extended than few kilometers upstream in MER and LUN/GIH, respectively. This reduced time extents are probably due to the location of these stations near the slopes and not in the center of the valleys. The vicinity of the lake ($<$ 100 m) can also cause this difference at the BRZ station due to its higher thermal inertia.

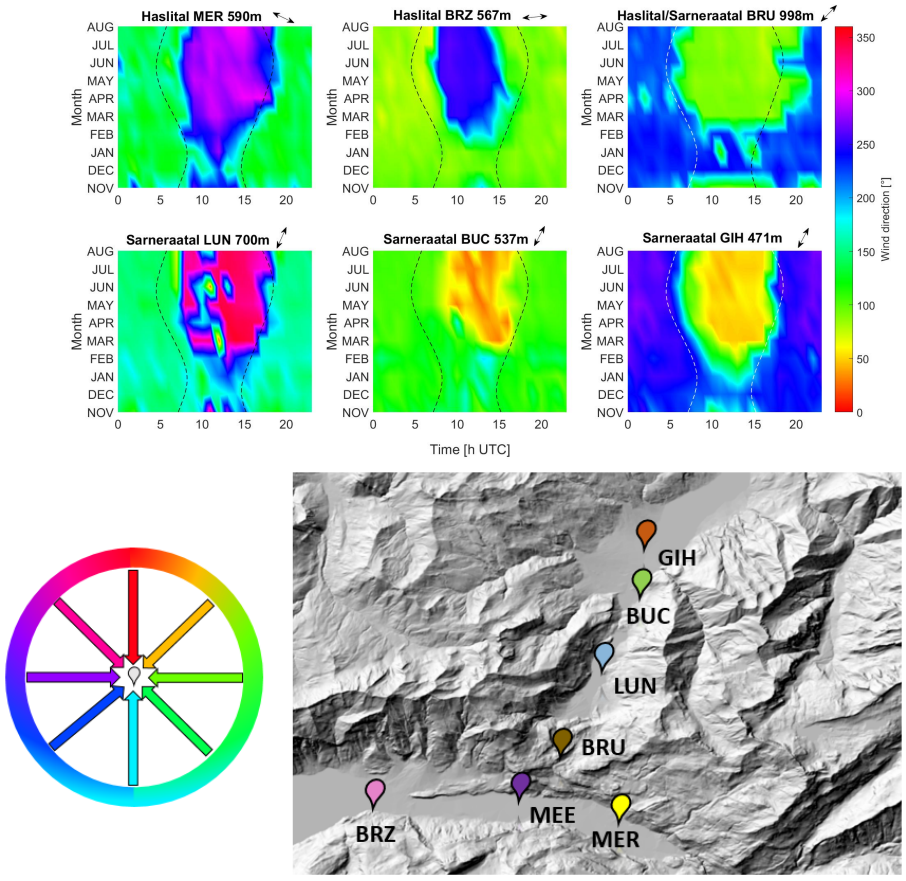

Figure S10. Monthly median wind direction [°] at ground level for the different automatic measurement station of the Haslital (top row) and Sarneraatal (bottom row). The color code for wind direction is presented on the color wheel and the dashed lines correspond to sunrise and sunset times. The map was download from swisstopo (/https://map.geo.admin.ch, last access: 19.09.2023)

S11 T comparison during foehn

The effect of foehn on T is variable: during March 20, the foehn event started at 23:00 and inhibited the formation of the T inversion by destroying the stable layer built so far. This induced mild T during the night compared to previous days (S11, Fig. S11.a). On the other hand, for the event of March 11 and April 23, the foehn events start around 11:00, and the T increase is not as important. For March 11, the foehn breakthrough happens at 11:00 with a T increase of 8 °C between 08:00 and 09:00 and a second T increase of 3 °C between 11:00 and 12:00. The MWR measures the same T evolution. With a delay of less than an hour, KENDA at MEE and MER (Fig. S11.b-c) show the same temporal T evolution as at SMN. However, the temporal T gradients are smaller because of the missed inversion of the previous night and the underestimated T during the foehn event. The two modeled T evolution exhibits a delay of one hour. KENDA-1/MER T increase happens before that from MEE which is coherent with the orientation of the Haslital and the provenance of foehn. For the rest of the profile, the rapid T increase is observed between the ground and 1200 m and nearly constant T are measured in that part of the profile. KENDA-1 shows the same pattern with a negative T bias of 2 °C that grows up to 4°C when maximal wind speed is reached. For March 20, at ground, the foehn breakthrough at 11:00 breaks the inversion around midnight and maintains mild T until the arrival of the sun where the T further rise according to a classical daily cycle. KENDA-1 ground T at MER and MEE does not show any T increase during

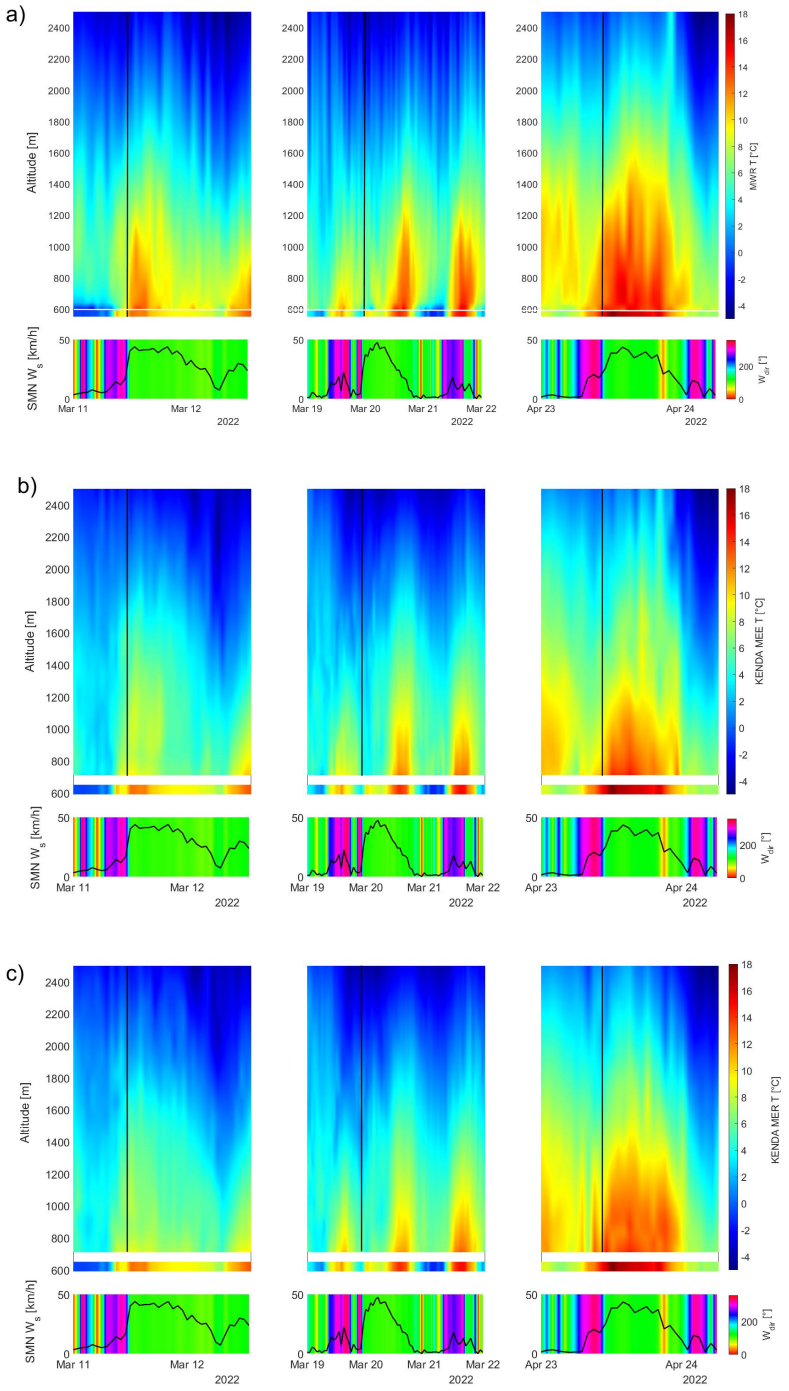

Figure S11. T profiles [°C] timeserie from a) MWR b) KENDA-1 MEE and c) KENDA-1 MER. during a selection of 3 foehn events during the campaign: left 11-12.03.2022, middle 19-22.03.2022 and right 23.04.2022. T, wind speed [km/h] and direction [°] from the SMN MER are given in the lower part of each figure. The solid line represent the begining of the foehn event.

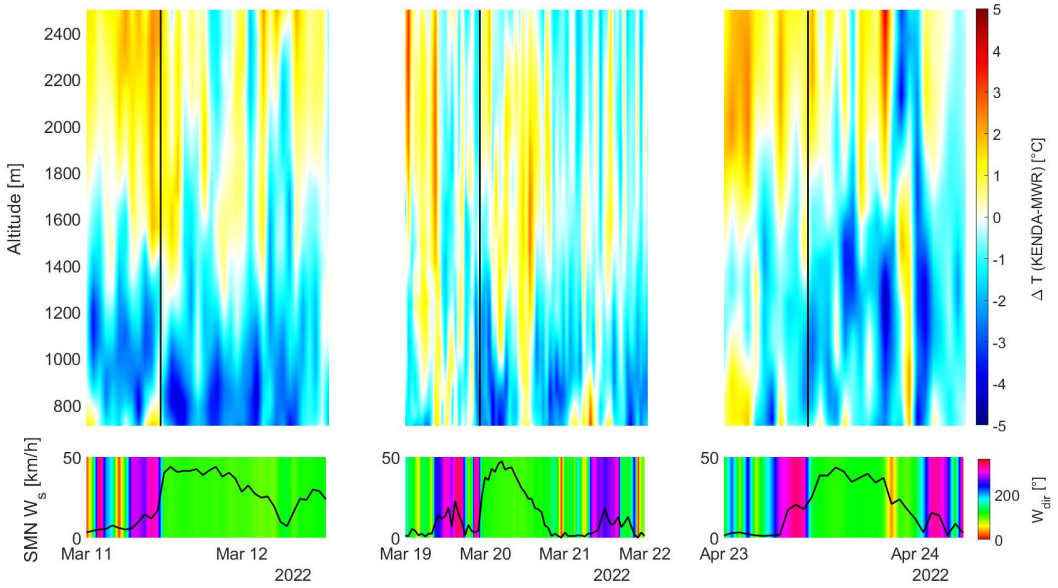

Figure S12. T profiles comparison [°C] between KENDA-1/MEE and MWR/MEE during a selection of 3 foehn events during the campaign: left 11-12.03.2022, middle 19-22.03.2022 and right 23-24.04.2022. Wind speed [km/h] and direction [°] from the SMN MER are given in the lower part of each figure. The solid line represent the begining of the foehn event.

the night and therefore underestimates the T. During daytime, the T underestimation is the same as for days without foehn. For the rest of the profile, the T are better modeled than for the 11.03. The T underestimation (2-3 °C) again extends from ground to 1200 m but this time it remains only in the first 4 hr of the event. Afterward, this underestimation is constrained under 900 m. Finally for the 24th of April, at ground, MWR and SMN T are the same until the foehn breakthrough at 11:00. The two measurements then show a 2 °C difference during the foehn event (wind speeds $>$ 25km/h). KENDA MEE and MER are similar to the MWR measurements. For the rest of the profile, the model is again underestimating the T but higher up, between 1200 and 1400 m.

S12 Wind speed and direction comparison during foehn

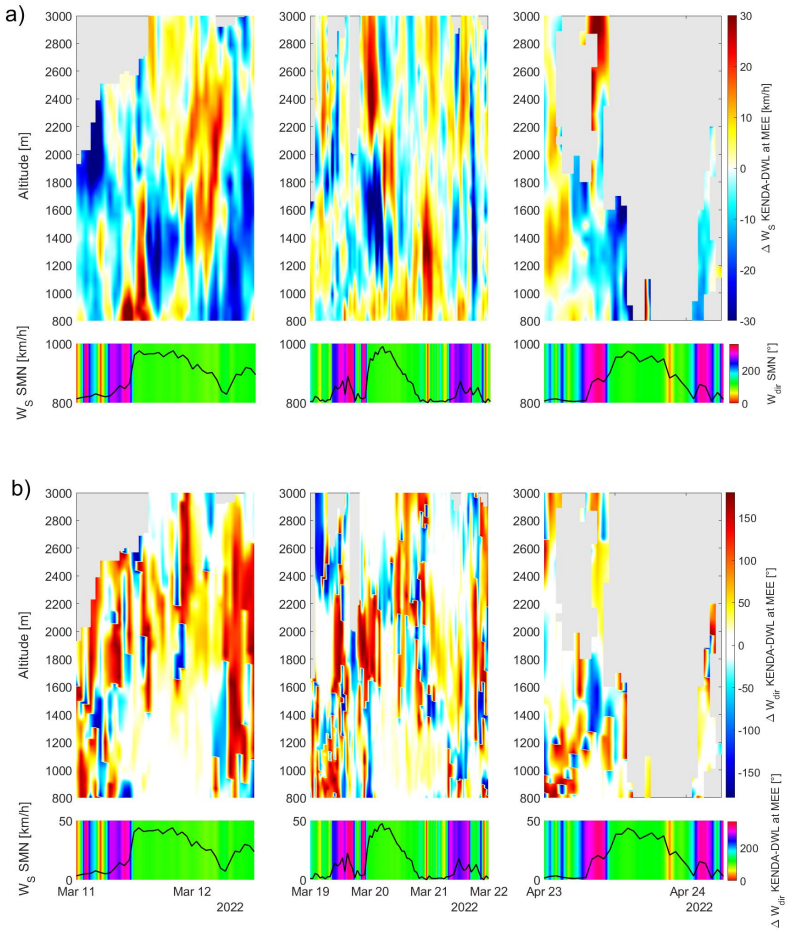

Figure S13. a) Wind speed [km/h] and b) wind direction [°] differences between KENDA-1/MEE and DWL/MEE profiles during a selection of 3 foehn events: left 11-12.03.2022, middle 19-22.03.2022 and right 23-24.04.2022. Wind speed [km/h] and direction [°] from the SMN MER are given in the lower part of each figure.